Available online at www.sciencedirect.com
ScienceDirect
Colloids and Surfaces A: Physicochem. Eng. Aspects 290 (2006) 41–49
COLLOIDS AND SURFACES A
www.elsevier.com/locate/colsurfa

Effect of wetting conditions and flow rate on bubble formation at orifices submerged in water

G. Corchero *, A. Medina, F.J. Higuera

ETS Ingenieros Aeronáuticos, Universidad Politécnica de Madrid, Plza. Cardenal Cisneros 3, 28040 Madrid, Spain

Received 24 June 2005; received in revised form 17 April 2006; accepted 25 April 2006
Available online 5 May 2006

Abstract

An experimental investigation has been carried out on the generation of bubbles due to the injection of a constant flow rate of air through an orifice submerged in water. Orifices of different radii drilled in horizontal plates of different materials, both hydrophilic and hydrophobic, have been used to cover a range of static contact angles ($68^\circ \leq \theta_0 \leq 123^\circ$), and a wide range of volumetric gas flow rates ($0.5\,\text{mm}^3/\text{s} \leq Q \leq 1.33 \times 10^4\,\text{mm}^3/\text{s}$) has been investigated. It is shown that data for different static contact angles and orifice radii can be approximately reduced to a single bubble volume/flow rate relationship when a properly scaled bubble volume at detachment is plotted versus a properly scaled volumetric gas flow rate. This data reduction permits an easy estimation of the bubble volume for any constant volumetric gas flow rate.

Keywords: Bubbles; Multiphase flow; Wettability; Contact angle; Bubble detachment

1. Introduction

The growth and detachment of gas bubbles in a liquid can occur in a variety of ways depending on the purpose and the actual conditions of the bubble formation process [1–4]. The bubbles can arise spontaneously in single- or multiple-component systems when boiling or cavitation nucleates them [4,5], or they can be generated by the injection of a gas flow through a needle or an orifice on a solid wall [1–3,6–15]. In some cases, the liquid partially wets the solid surface around the orifice, and this partial wetting influences the shape of the bubbles attached to the orifice, the radius of their contact line, and their volume at detachment. This effect has been observed both for bubbles growing in supersaturated liquids [4] and in orifice-plate configurations [13–18], typically when the static contact angle θ_0 varies from values larger than 90° (hydrophobic surfaces) to smaller than 90° (hydrophilic surfaces).

Knowledge of how wettability affects the growth and detachment of the bubbles is important in many applications [4,13–19]. A case in point is gas sparging in metallurgical operations at high temperature, in which tuyeres are commonly used to control the injection of a gas into a vessel where the molten metal is gradually cleaned. The mouth of each tuyere is surrounded by a refractory solid, which is only partially wetted by the molten metal. The gas bubbles spread over the surface of this solid during their growth process, and large non-spherical bubbles are generated with volumes up to twice the volume of the bubbles in systems where the liquid wets perfectly the solid. Gerlach et al. [18] predict that the volume increases by a factor of 2.34 when the static contact angle changes from 90 to 120° for an injection orifice radius of 1 mm; see Table 1. Experimental data on these large bubbles have been gathered for systems such as Argon-pig iron-alumina, for which the contact angle varies from 130 to 64° when the oxygen content of the iron changes from 60 to 460 parts per million (ppm) [13]. The effect of the contact angle has been accounted for in theoretical models for surface tension-dominated and inertia-dominated regimes [6,17,18,20]. It is worth noticing that the complex systems found in metallurgical operations and in other cases are equivalent to simple air-water-plastic systems at ambient temperature when the Bond number, $B = \rho g a^2/\sigma$, the Weber number, $\text{We} = \rho Q^2/\sigma a^3$, and the static contact angle, θ_0, are equal in both systems. Here ρ and σ are the density and surface tension of the liquid, Q the volumetric flow rate of gas, a the radius of the injection orifice, and g the acceleration due to gravity. This equivalence has enormous consequences if one compares the easy visualization of air bubbles

* Corresponding author. Tel.: +34 91 3366352; fax: +34 91 3366375.
E-mail address: corchero@aero.upm.es (G. Corchero).

0927-7757/$ – see front matter © 2006 Elsevier B.V. All rights reserved.
doi:10.1016/j.colsurfa.2006.04.046

Nomenclature

a	radius of the injection orifice
$B = \rho g a^2/\sigma$	bond number
g	gravity acceleration
P	pressure
p_c	capillarity pressure
Q	volumetric flow rate through the injection orifice
Q, $\tilde{Q}_{cr}$, Q'_{cr}	volumetric flow rate scaling factors
R_b	radius of the contact line
R_{bmax}	maximum radius of the contact line
V	volume of the attached bubble
V_b	volume of the bubble at detachment
$\tilde{V}_F$, V_F, V'_F	volume scaling factors
$We = \rho Q^2/\sigma a^3$	Weber number
ϕ	diameter
μ	dynamic viscosity of the liquid
ρ	density of the liquid
θ_0	static contact angle
θ	contact angle
σ	surface tension

Subscripts

cap	capillary
cr	critical value
F	Fritz
fl	feed line
G	gas
of	orifice
T	teflon
V	vaseline

in water with the difficulties inherent to opaque molten metals. The equivalence also opens a path to analyse some heat and mass transfer processes, which are determined to a large extent by the bubble volume and the frequency of bubble detachment.

The influence of the air injection conditions on bubble growth and detachment has been also extensively discussed in the literature [1–3,7,8,12,13,17]. A constant volumetric flow rate has been often assumed, but this condition is not always easy to achieve. Analysis of the reported evolution of the bubble volume in some nominally constant flow rate experiments shows that the actual volumetric flow rate is not constant in an initial step of the bubble growth process, which may represent about one-fourth or one-third of the total time of growth [9,10,13–15,17] and may have an important influence on the whole bubble formation process [1,2,12]. Ideally the radius of the bubble decreases in an initial step from very large values to a minimum of the order of the orifice radius a, and then increases again [12]. This evolution of the radius leads to a maximum overpressure in the bubble of the order of $p_c = 2\sigma/a$, and it is well-known that irregularities, promoting coalescence at the injection orifice and random generation of bubbles, tend to appear when pressure variations of the order of p_c can influence the air flow rate through the injection orifice [11,12].

The purpose of this work is to analyse the process of bubble formation at submerged orifices in hydrophilic, neutral ($\theta_0 = 90°$), and hydrophobic surfaces for a wide range of constant flow rates. We have devised for this purpose an experiment that allows to generate a constant and controlled flow rate of air in the range from 0.5 to 1.33×10^3 mm^3/s through a circular orifice of given radius in the range from 0.5 to 1 mm. This orifice is drilled at the horizontal bottom wall of a reservoir filled with water at rest. Three different values of the static contact angle have been investigated in the range $68° \leq \theta_0 \leq 123°$. Previous work along these lines includes the papers of Gnyloskurenko et al. [14] and Byakova et al. [15]. The work of [14] covers the range of contact angles $68° \leq \theta_0 \leq 110°$, focusing on a single value of the gas flow rate, $Q = 33$ mm^3/s, with $B = 3.4 \times 10^{-2}$ and $We = 0.12$. The work of [15] covers the range $15° \leq \theta_0 \leq 110°$ and narrow ranges of We and B. Both works report complex behaviour during bubble formation and, in both cases, the flow rate has a certain time variation during the bubbling period, which apparently affects the final volume of the bubbles.

The paper is organized as follows. The experimental setup, the data acquisition procedures, and the procedures used to measure the growth and formation of the bubbles are described in Section 2. The experimental results are presented in Section 3, and a scaling analysis that extends the well-known theory of Davidson and Schuler [7] to account for bubbling from an orifice in neutral ($\theta_0 = 90°$) and hydrophobic ($\theta_0 > 90°$) surfaces is presented in Section 4. The main conclusions of the work are summarised in Section 5.

2. Experimental study

2.1. Experimental setup

Bubbles were generated by injecting a constant volumetric flow of air through a circular orifice drilled at the center of the

Table 1
Available values of some key variables from previous works

θ (°)	a (mm)	R_{bmax} (mm)		V_b (mm^3)		Q (mm^3/s)	References
		Experiments	Predicted	Experiments	Predicted		
90	0.5	1.3	–	32.13	–	33.33	[14,15]
110	0.5	2.5	–	62.86	–	33.33	[14,15]
90	0.5	–	2.50	–	69.25	–	[18]
108	1	2.7	3.53	–	119	166.66	[18]
94	1.8	4.25	–	–	–	1100	[13]
130	1.2	3.25	–	–	–	1100	[13]

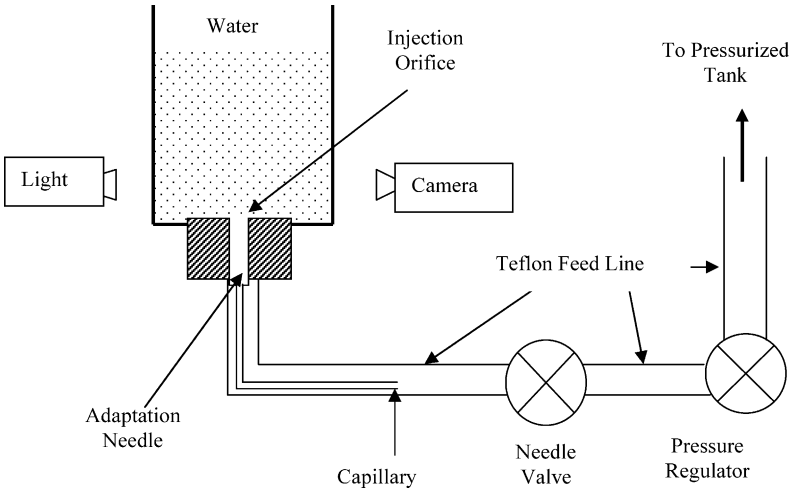

Fig. 1. Sketch of the experimental setup.

base of a vertical reservoir of 5 cm × 5 cm square cross section and 10 cm high, which is filled with water at rest to a height of 5 cm above the injection orifice. The air is injected vertically.

Fig. 1 is a sketch of the experimental setup. The air flows from a pressurized tank through a pressure reduction valve and a needle valve into a closed teflon tube and then into a stainless steel capillary, which is used to feed the injection orifice with air through a short needle of the same radius as the injection orifice and length $l_{of} = 40$ mm. The purpose of the capillary is to ensure that the volumetric flow rate of air is a constant by imposing a pressure drop very large compared with the pressure variations elsewhere in the system. The Teflon tube has a length of 10 m and an inner diameter $\phi_T = 2$ mm, while the stainless steel capillary has a length $l_{cap} = 2.3$ m, an inner diameter $\phi_{cap} = 0.35$ mm, and an outer diameter of 0.5 mm. The criterion used to determine the length of the capillary is discussed in the following subsection. The pressure at the inlet of the capillary can be varied from 6 kg/cm^2 to the atmospheric pressure by means of the control valves.

The radius of the injection orifice was varied from 0.5 to 1.0 mm. The base of the water reservoir was made out of acrylic or machinable teflon plates with static contact angles $\theta_0 = 68$ and 123°, respectively. In another series of experiments, the base was coated with domestic vaseline, which changes the static contact angle to $\theta_0 = 90°$. Values of the water density and surface tension are $\rho = 1000$ kg/m^3 and $\sigma = 0.073$ N/m. The experiments were carried out at room temperature.

The bubble growth and detachment were video recorded with a high speed, digital video camera, model Redlake 8000S, which may record up to 8000 images per second. The video sequences were analysed off line to compute the shape, center of mass and volume of each bubble with an error of 2%.

2.2. Length of the capillary

The procedure to ensure a constant volumetric flow rate, or at least to guarantee that the flow rate is not influenced by the bubble formation process, is to impose a pressure drop in the feeding line upstream of the injection orifice much larger than the pressure variation in the bubble, of order $p_c = 2\sigma/a$. This idea was suggested in previous works [1,2,8,12].

The pressure drop in each of the tubes of our system can be computed in terms of the flow rate Q using Poiseuille's formula

$$Q = \frac{\pi}{128}\frac{\phi^4}{\mu_G}\frac{\Delta P}{l}, \tag{1}$$

where μ_G is the dynamic viscosity of the gas, l and ϕ the length and inner diameter of the tube, and ΔP the pressure drop along the tube. When expression (1) is applied to the capillary, it gives the pressure drop in the capillary ΔP_{cap} as

$$\Delta P_{cap} \approx \frac{128}{\pi}\frac{\mu_G l_{cap}}{\phi_{cap}^4} Q, \tag{2}$$

where l_{cap} and ϕ_{cap} are the length and inner diameter of the capillary. We have determined the length of the capillary by imposing the condition

$$\frac{\Delta P_{cap}}{(2\sigma/a)} \geq 100 \tag{3}$$

at the smallest flow rate of interest. This condition ensures that the bubble growth process does not significantly influence the volumetric flow rate.

The pressure drop ΔP_{fl} from the exit of the control valves to the exit of the injection orifice can be expressed as

$$\Delta P_{fl} = \Delta P_{cap} + \Delta P_{of} + \Delta P_T, \tag{4}$$

where ΔP_{of}, ΔP_T and ΔP_{cap} are the pressure drops through the adaptation tube, the teflon tube and the capillary, respectively. Using (1) to evaluate each pressure drop, we find

$$\frac{\Delta P_{of} + \Delta P_T}{\Delta P_{cap}} = \frac{l_{of}}{l_{cap}}\left(\frac{\phi_{cap}}{2a}\right)^4 + \frac{l_T}{l_{cap}}\left(\frac{\phi_{cap}}{\phi_T}\right)^4, \tag{5}$$

which takes a value of 0.004 in our experimental setup. This means that the volumetric flow rate through the injection orifice is controlled by the pressure drop in the capillary, and expression (2) can be used with an expected error of 0.4%

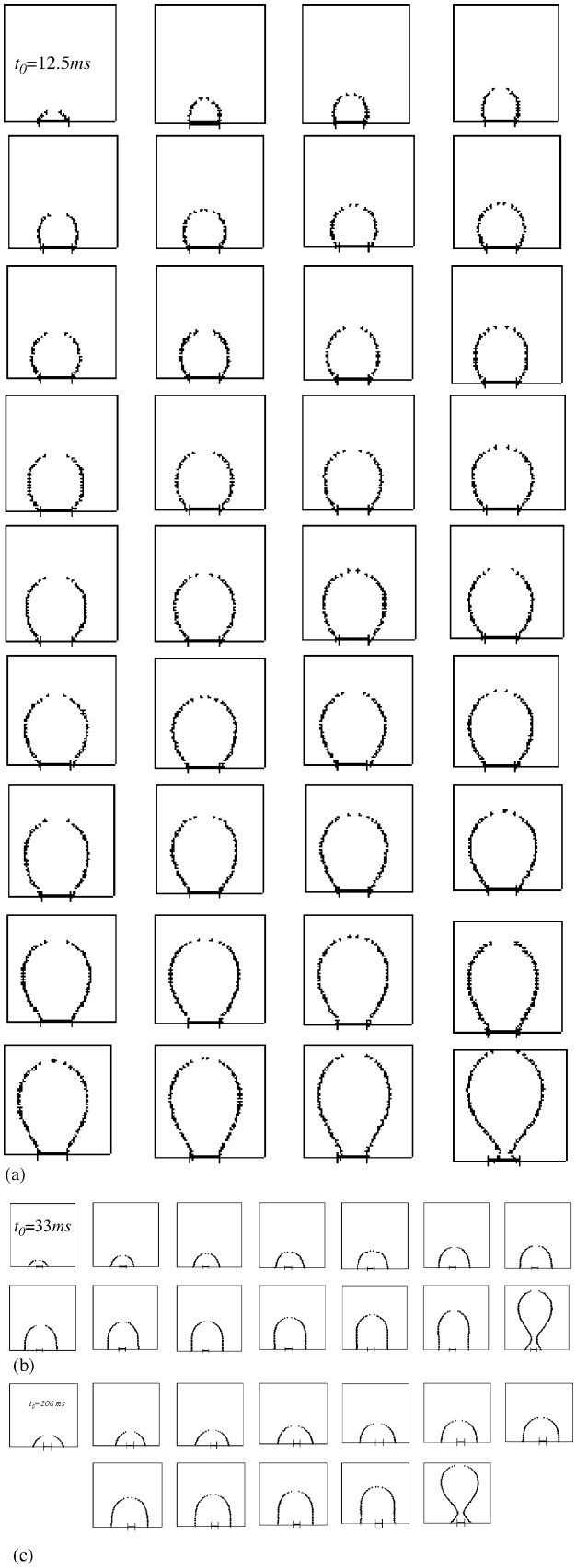

Fig. 2. Time variation of the bubble profile during the bubbling process. (a) Acrylic plate, $a = 0.5$ mm, $\theta_0 = 68^\circ$, $Q = 48.4$ mm^3/s, $\Delta t = 12.5$ ms, $t_0 = 12.5$ ms. Δt and t_0 are the time between two consecutive frames and the time to the first shown frame, respectively; (b) teflon plate, $a = 0.5$ mm, $\theta_0 = 123^\circ$, $Q = 60.2$ mm^3/s, $\Delta t = 100$ ms, $t_0 = 33$ ms; (c) vaseline substrate, $a = 0.5$ mm, $\theta_0 = 90^\circ$, $Q = 57.9$ mm^3/s, $\Delta t = 125$ ms, $t_0 = 208$ ms.

2.3. Measurement procedure

The camera records digital images whose size depends on how fast is the flow. For low flow rates typical images have 480×420 pixels, while for moderate flow rates the size is 160×140 pixels. A simple filtering process is enough to extract the contour of the bubble when the illumination intensity and the camera shutter speed are properly adjusted. An object of known size is located in the vicinity of the injection orifice and serves as a measurement scale on the video pictures. The spatial resolution of the pictures was 0.1 mm/pixel or better in all the experiments. Linear interpolation of luminosity between adjacent pixels was used to determine the contour of the bubble. The goodness of this procedure is evidenced in Fig. 2, which shows a few discretized contours of bubbles on each of the three surfaces. Assuming the bubbles are axisymmetric, an ad hoc numerical code is used to measure their volume V_b, their center of mass, and the radius of the contact line R_b as functions of time, as well as the volume of the bubble at detachment.

The static contact angle θ_0 for each air–solid–water system was measured using the sessile drop method after the solid surface was drilled and smoothed. The first two points on the discretized contour were used to draw the tangent. Since the contour was discretized using all the pixels in the video images, the distance between these two points was about 0.1 mm, and the distance from the solid surface to first point was always less or equal than 0.1 mm.

3. Results

Fig. 2 shows three series of snapshots during the growth of a bubble at three different surfaces with nearly equal values of the volumetric flow rate: (a) $Q = 48.4$ mm^3/s for acrylic surface; (b) $Q = 60.2$ mm^3/s for teflon surface; and (c) $Q = 57.9$ mm^3/s for vaseline substrate. The orifice is marked by two vertical tics in all cases. Fig. 3 shows the evolution of the bubble volume, the radius of the contact line R_b, and the contact angle θ, during the formation process for the cases shown in Fig. 2. The magnitudes R_b and θ are shown only for cases (b) and (c), where their values are relevant.

The data for the bubble volume in Fig. 3 accurately fall on straight lines, which proves that the injection system provides a constant volumetric flow rate of air through the injection orifice, i.e. $Q = dV/dt = \text{constant}$, for hydrophilic, neutral, and hydrophobic surfaces. The first point in Fig. 3a, for the case of an hydrophilic surface, is located very close in time to the condition of maximum capillary pressure; see Fig. 2a and Section 1. The bubble volume cannot be measured in an initial step of the bubble growth because it is not possible to discriminate

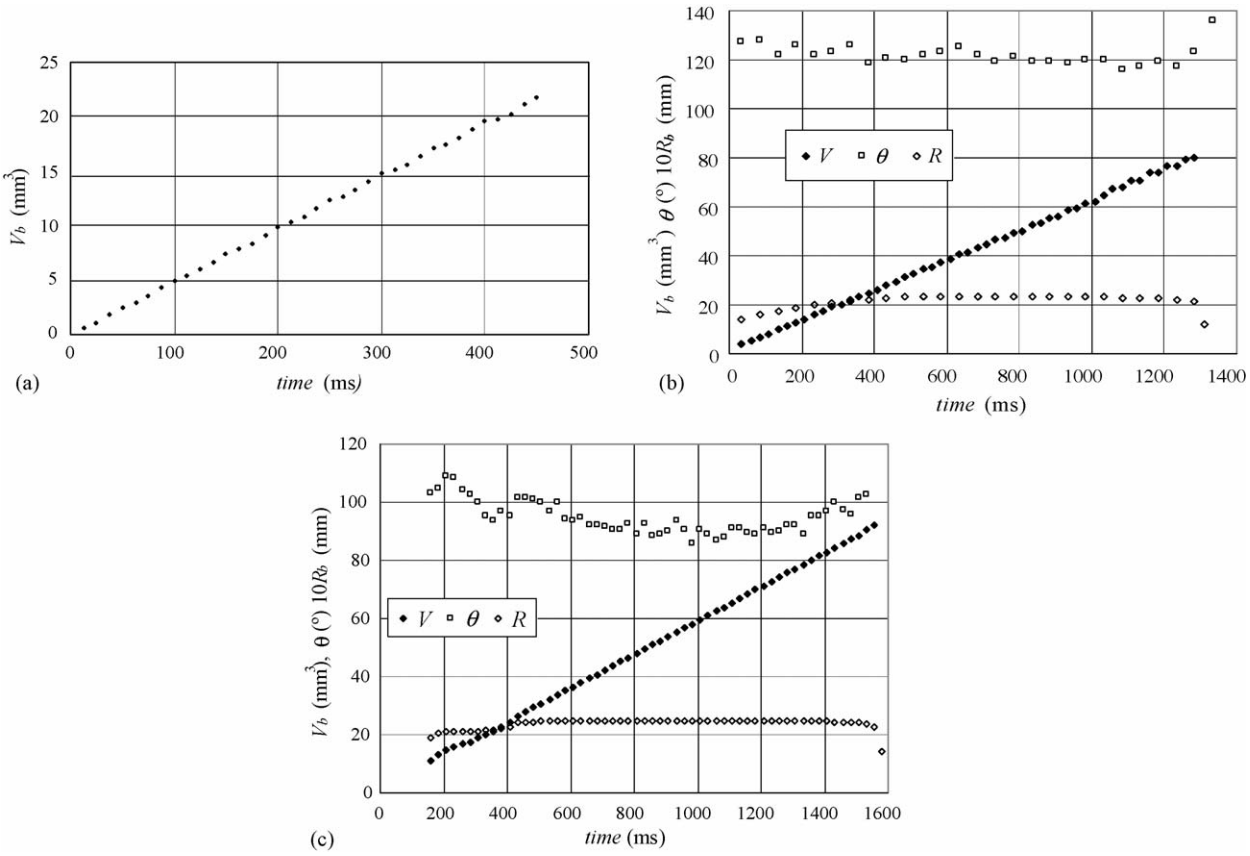

Fig. 3. (a) Variation of the bubble volume during the growth process. Acrylic plate, $a = 0.5$ mm, $\theta_0 = 68°$, $Q = 48.4$ mm^3/s; (b) variation of some characteristic magnitudes of the bubble during the bubbling process. Teflon plate, $a = 0.5$ mm, $\theta_0 = 123°$, $Q = 60.2$ mm^3/s; and (c) variation of some characteristic magnitudes of the bubble during bubbling process. Vaseline substrate, $a = 0.5$ mm, $\theta_0 = 90°$, $Q = 57.9$ mm^3/s.

the bubble profile, but this step represents only 2–3% of the total bubbling period. Tsuge [8] stated that a capillary aids to achieve a constant volumetric gas flow rate by overcoming the pressure fluctuations that appear during the bubble formation, when the length of the capillary is larger than $10^6\phi_{cap}$. This criterion would give l_{cap} >350 m in our case, but the results of Fig. 3 shows that a much shorter capillary suffices to achieve a constant gas flow rate and a periodic regime of bubble generation (thus avoiding the problem of bubble generation in groups which has been reported in several works [11,12]). The result $V = Qt$ is in agreement with ref. [17], which states that the assumption of bubble volume growth equal to the gas flow rate is adequate for very small chamber volumes (here this volume is zero).

Fig. 2a shows that the contact line of the bubble with the solid coincides with the edge of the orifice when $\theta_0 = 68°$. In this case the volume of the bubble increases with time while it keeps anchored to the edge of the orifice. Buoyancy forces dominate surface tension in a final stretching process, just before detachment, in which the part of the bubble surface below the neck moves inside the orifice (see last frame in Fig. 2a). This sequence has been described in the literature for the case of hydrophilic surfaces ($\theta_0 < 90°$); see ref. [17].

Fig. 2b and c, for a hydrophobic surface ($\theta_0 = 123°$) and a neutral surface ($\theta_0 = 90°$), respectively, show that the radius of the contact line R_b is larger than the radius of the orifice (again marked by two vertical tics) at any time during the process. There are three steps in the evolution of the bubble. The bubble is fairly round and the contact line shifts outward in a short initial step. This is followed by a longer second step in which the bubble is approximately a vertical cylinder of constant radius R_{bmax} and increasing height capped by a semi-sphere. When the height of this cylinder is about equal to or a little larger than its radius, the buoyancy force stretches very quickly the bubble and causes its detachment in a short third step during which the contact line recedes toward to the injection orifice. The third step covers about 10% of the bubbling period. The growth process of the bubble is similar in Fig. 2b and c up to obvious differences around the contact line, and it is also very similar to the growth process reported in ref. [18] for $\theta_0 = 108°$.

Fig. 3b and c show that the radius of contact line R_b has only slight variations during the bubble formation process for static contact angles of 123° (teflon) and 90° (vaseline substrate). In addition, the measured contact angle θ reaches the static contact angle θ_0 very early in the evolution of the bubble, stays practically constant at θ_0 during most of the process, and increases very rapidly in the final stretching step immediately before detachment. The dependence of the contact angle on the velocity of the contact line, including effects of hysteresis, is discussed in refs. [21,22], among others. It seems, however, that those complex effects do not play an important role in our experiments, probably due to the limited variation of R_b with time (see also ref. [18]).

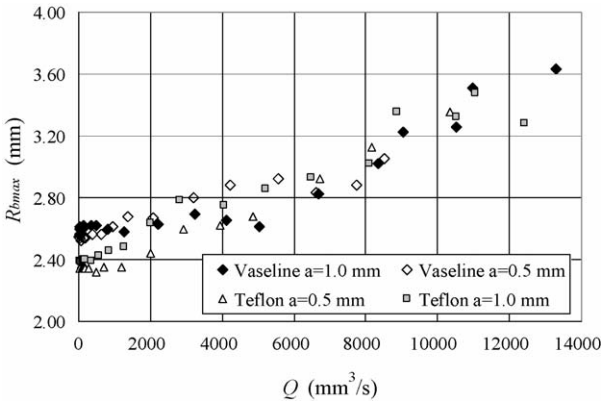

Fig. 4. Maximum radius of the contact line R_{bmax} vs. volumetric flow rate for all studied radii, for neutral ($\theta_0 = 90°$) and hydrophobic ($\theta_0 = 123°$) surfaces.

Fig. 4 shows the maximum radius of the contact line R_{bmax} as a function of the volumetric flow rate for neutral (vaseline) and hydrophobic (teflon) surfaces. The data in this figure cover a wide range of flow rates ($0.5\,\text{mm}^3/\text{s} \le Q \le 1.33 \times 10^4\,\text{mm}^3/\text{s}$) and show that the values of R_{bmax} for different runs, including neutral and hydrophobic surfaces and different injection radii, nearly coincide for flow rates above approximately $10^3\,\text{mm}^3/\text{s}$. These results confirm therefore that the influences of the static contact angle and the injection radius are essentially low flow rate effects that tend to disappear when the flow rate increases. The region of low flow rates will be further discussed in Section 4.

Results similar to those of Fig. 4 have been obtained by Liow and Gray [13] in experiments on bubble growth in Argon-alumina-pig iron as the gas–solid–liquid system, where the liquid density and surface tension are $\rho = 700\,\text{kg/m}^3$ and $\sigma = 1.265\,\text{N/m}$. In the experiments of ref. [13] a constant volumetric flow rate of gas in the range $2 \times 10^3\,\text{mm}^3/\text{s} \le Q \le 1 \times 10^6\,\text{mm}^3/\text{s}$ is injected through an orifice of radius $a = 3.175 \times 10^{-3}\,\text{m}$. This leads to $B = 0.54$ and a Weber number in the range $0.069 \le \text{We} \le 17289$. For comparison, our experiments with bubbles of air in water at ambient temperature cover the ranges $0.04 \le B \le 0.13$ and $3.47 \times 10^{-6} \le \text{We} \le 663$, with static contact angles of 68, 90 and 123°.

4. Discussion

Much work has been devoted to the analysis of the growth and detachment of bubbles from needles, where the wetting conditions are not so significant as when the orifice is drilled in a horizontal wall [1–3,7,8,12]. It is well-known that the bubbles grow quasistatically at the tip of a needle through which a small volumetric flow rate is injected, following a sequence of equilibrium shapes with increasing volume. The equilibrium shapes are spheres when the Bond number is also small, in which case the volume of a bubble at detachment V_F can be determined from the balance of buoyancy and surface tension forces: $\rho g V_F = 2\pi a \sigma$, where the density of the air ρ_G has been neglected compared to the density of the liquid. This balance yields

$$V_F = \frac{4}{3}\pi R_F^3 \quad \text{with} \quad R_F = \left(\frac{3}{2}\frac{\sigma a}{\rho g}\right)^{1/3}, \tag{6}$$

which are the Fritz volume V_F and radius R_F [23]. Notice that $V_F/a^3 = 2\pi/B$ is a large quantity.

Oguz and Prosperetti [12] carried out a numerical and experimental analysis of the problem of bubble generation from a needle, and concluded that the relation between the bubble volume at detachment and the gas flow rate is universal when the volume is scaled with the Fritz volume V_F and the flow rate is scaled by a critical flow rate Q_{cr} given by

$$Q_{cr} = \left(\frac{\pi}{6}\right)^{1/6} g^{1/2} V_F^{5/6}. \tag{7}$$

According to ref. [12], V_b/V_F is a constant when $Q/Q_{cr} \ll 1$ and increases as $(Q/Q_{cr})^{6/5}$ when $Q/Q_{cr} \gg 1$. The critical volumetric flow rate Q_{cr} represents an upper bound of the range of flow rates where the quasistatic approximation is reasonable.

The results for small Q/Q_{cr} reviewed here should be valid also for bubbles issuing from a circular orifice at the bottom wall of a liquid if the contact line coincides with the edge of the orifice at the instant of detachment. This is the case when the liquid wets the surface with a small contact angle, but not for the neutral ($\theta_0 = 90°$) and hydrophobic ($\theta_0 = 123°$) surfaces investigated in this work. In the latter cases the contact line drifts away from the edge of the orifice and its radius is of the order of the size (cubic root of the volume) of the bubble, which is large compared with the radius of the orifice if $B \ll 1$. The Bond number based on the size of the bubble is not small, and the bubble is not spherical. To see to what extent the classical theory for injection from a needle can be extended to deal with these conditions, and guided by previous comments of Gnyloskurenko et al. [14], we introduce here modified scales Q'_{cr} and V'_F, by using (6) and (7) with the radius of the orifice replaced by the maximum radius of the contact line R_{bmax} measured during the growth of a bubble at very small volumetric flow rates. The measured V_b/V'_F is plotted in Fig. 5 versus the measured Q/Q'_{cr}, for hydrophilic, neutral and hydrophobic surfaces. As can be seen, the experimental data fall approximately onto a single curve when this modified scaling is used, not only for small values of Q/Q'_{cr} but also when this parameter is moderately large. In fact, the same

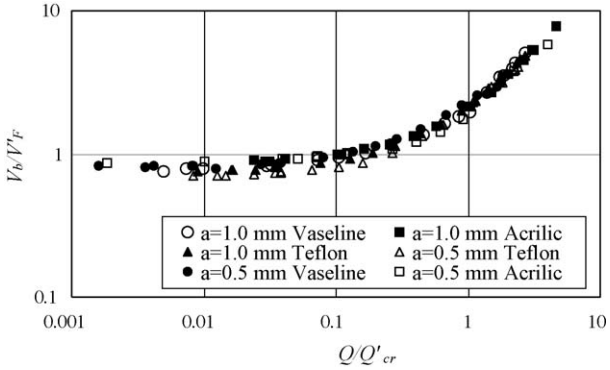

Fig. 5. Nondimensional volume at detachment V_b/V'_F vs. the nondimensional volumetric flow rate Q/Q'_{cr} for all the cases studied.

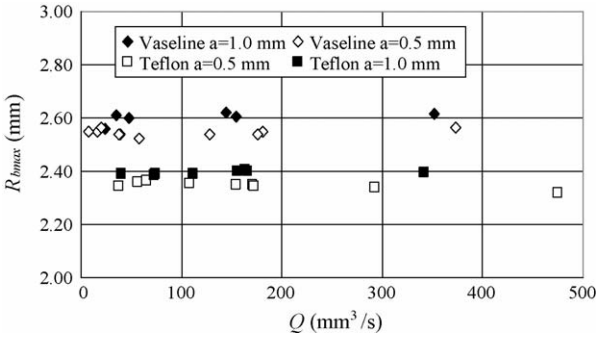

Fig. 6. Maximum radius of the contact line R_{bmax} vs. volumetric flow rate ($Q < 500\,mm^3/s$) for all studied radii, for neutral ($\theta_0 = 90°$) and hydrophobic ($\theta_0 = 123°$) surfaces.

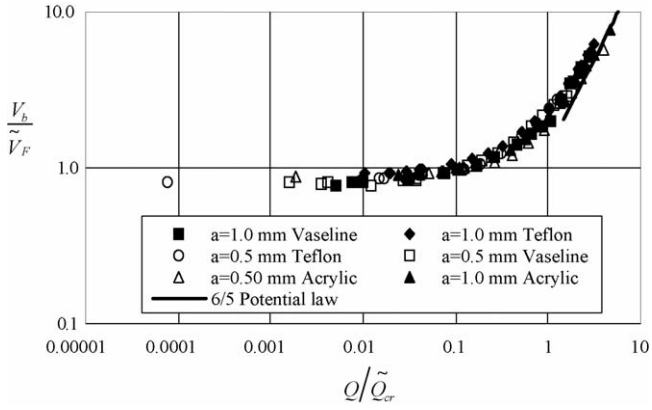

Fig. 7. Scaled volume at detachment $V_b/\tilde{V}_F$ vs. the scaled volumetric flow rate $Q/\tilde{Q}_{cr}$ for all studied radii, for hydrophilic ($\theta_0 < 90°$), neutral ($\theta_0 = 90°$) and hydrophobic ($\theta_0 = 123°$) surfaces.

three regions discussed by Oguz and Prosperetti [12] for the case of injection from a needle are apparent in Fig. 5. Namely, a region for low Q/Q'_{cr} where the dimensionless volume V_b/V'_F is practically constant and independent of the dimensionless flow rate; an asymptotic region for $Q/Q'_{cr} >> 1$; and an intermediate region where buoyancy, surface tension and inertia effects are important.

The collapse of experimental data in Fig. 5 is encouraging, but this figure is not easy to use in practice because it requires an independent measurement of R_{bmax} for the gas–solid–liquid system of interest in the cases of neutral and hydrophobic surfaces. It is only for hydrophilic surfaces that the maximum bubble base radius coincides with the orifice radius that the classical theory is recovered.

To try to overcome this difficulty, we propose here a coarse estimate of R_{bmax} based on the experimental results of the previous section for small flow rates ($Q < 500\,mm^3/s$). These results show that (i) the maximum radius of the contact line R_{bmax} is a function of the static contact angle θ_0 and is nearly independent of the radius of the injection orifice (see Fig. 6, which is a closeup of the lower part of Fig. 4); and (ii) the contact angle θ and the radius of the contact line of the bubble R_b very rapidly approach the static contact angle θ_0 and the maximum radius of the contact line R_{bmax}, respectively, and stay nearly constant at these values during most of the quasistatic evolution of an attached bubble (see Fig. 3b and c). The volume of the bubble at the end of its quasistatic evolution is a good approximation to the final volume at detachment, because the final stretching and necking process, which is not quasistatic, is very short (about 10% of the bubbling period as it was mentioned above). In addition, the snapshots of Fig. 2 show that the shape of the bubble at the end of the quasistatic evolution can be reasonably approximated by a cylinder of radius and height equal to its radius R_{bmax} capped by a semi-sphere of the same radius.

If these approximations are adopted, then the volume of the bubble at detachment is $\tilde{V}_F = (5/3)\pi R^3_{b\,max}$, and the equilibrium of buoyancy, air pressure, and surface tension forces that defines the end of the quasistatic evolution reads $\rho g \tilde{V}_F + \pi R^2_{bmax} \Delta P_b = 2\pi R_{bmax} \sigma \sin\theta_0$, which is a generalization of the original hydrostatic balance of Fritz [23] reviewed in the text above Eq. (6). Here, ΔP_b is the excess of pressure of the air in the bubble above the pressure of the liquid at the level of the orifice.

Kabanov and Frumkin [24] evaluate ΔP_b as the difference between the pressure jump across the surface due to surface tension at the tip of the bubble and the hydrostatic depression between the tip and the foot of the bubble, but this leads to $\tilde{V}_F = 0$ when $\theta_0 = 90°$ in our simple model of the bubble shape (for which [24] would give $\Delta P_b = 2\sigma/R_{bmax} - 2\rho g R_{bmax}$). To work out an alternative estimate of ΔP_b consistent with the rest of the model, we first approximate the surface of the bubble in the vicinity of the contact line by a cone of half angle $|\pi/2 - \theta_0|$. This approximation gives $\Delta P_b = \sigma \sin\theta_0 / R_{bmax}$, which decreases with θ_0 for values above 90°, consistently with the theoretical results of ref. [18]. If this ΔP_b is carried to the balance of forces of the preceding paragraph, then $\tilde{V}_F$ comes out much smaller than the experimental values of the bubble volume, which means that ΔP_b is overestimated. In fact, inspection of the bubble profiles of Fig. 2b and c shows that the curvature of the meridional sections displayed in these figures is not negligible (as it would be for a cone) and is opposite to the curvature of the cone tangent to the bubble. To take this second curvature into account we write $\Delta P_b = 2k\sigma \sin\theta_0 / R_{bmax}$, with k a constant to be determined by fitting the experimental results. Using this form of ΔP_b, the balance of the forces acting on the bubble gives

$$R_{bmax} = \left(\frac{6}{5} \frac{(1-k)\sigma \sin\theta_0}{\rho g} \right)^{1/2}, \tag{8}$$

which depends on the static contact angle and attains a maximum for neutral surfaces ($\theta_0 = 90°$), in line with the results of Figs. 3 and 6. If expression (8) is used now to compute $\tilde{V}_F = (5/3)\pi R^3_{b\,max}$ and this volume is used to replace V_F in (7), we end up with the modified scaling factors

$$\tilde{V}_F = 2\pi \left(\frac{6}{5} \right)^{1/2} \left(\frac{(1-k)\sigma \sin\theta_0}{\rho g} \right)^{3/2} \quad \text{and}$$

$$\tilde{Q}_{cr} = 2 \left(\frac{2 \times 3^3}{5^5} \right)^{1/12} \pi \left(\frac{(1-k)\sigma \sin\theta_0}{\rho g^{3/5}} \right)^{5/4}. \tag{9}$$

Fig. 7 shows that the dimensionless bubble volume $V_b/\tilde{V}_F$ as a function of the dimensionless flow rate $Q/\tilde{Q}_{cr}$ approximately falls onto a single curve for any wetting conditions when the

modified scales (9) are used for vaseline-coated ($\theta_0 = 90^\circ$) and teflon ($\theta_0 = 123^\circ$) surfaces with $k = 0.1$, and the classical scales (6) and (7) are used for the acrylic surface ($\theta_0 = 68^\circ$). The value $k = 0.1$ means that the contribution of ΔP_b to the force balance is about 10% of the contribution of the vertical component of the surface tension acting across the contact line. Values of R_{bmax} computed from (8) are within 10% of our experimental values for small flow rates. Changeover from (8) and (9) to (6) is indicated when $\tilde{V}_F = V_F$.

Fig. 7 displays the same three regions discussed above in connection with Fig. 5 but, contrary to that figure, the new representation does not require an independent measurement of R_{bmax}. The solid curve of Fig. 7 is the potential law

$$\frac{V_b}{\tilde{V}_F} = 1.25\left(\frac{Q}{\tilde{Q}_{cr}}\right)^{6/5}, \tag{10}$$

which recasts the well-known asymptotic expression of the volume for very large flow rates [7,12] in terms of our dimensionless variables. Notice that the factor $\sigma \sin\theta_0$ in (9) cancels out when $\tilde{V}_F$ and $\tilde{Q}_{cr}$ are carried to (10). The predicted volume of the bubble becomes independent of the surface tension and the contact angle when the flow rate is large, as should be expected.

It should be stressed that the variation of R_{bmax} and $\tilde{V}_F$ as powers of $\sin\theta_0$ in (8) and (9) is a consequence of the particular shape of the bubble assumed in the paragraphs above Eq. (8). While the assumed shape is reasonable in the conditions of our experiments, and our experimental results support the predicted decrease of R_{bmax} and $\tilde{V}_F$ with increasing θ_0 for hydrophobic surfaces (see Fig. 3b and c), it is still true that the dependence on θ_0 in (8) and (9) does not follow from first principles. As a further test of these results, average values for R_{bmax} have been computed from Fig. 6 for vaseline substrate, $(R_{bmax})_V = 2.566$ mm, and teflon, $(R_{bmax})_T = 2.360$ mm. The ratio $(R_{bmax})_V/(R_{bmax})_T = 1.087$ is in good agreement with the prediction $(R_{bmax})_V/(R_{bmax})_T = (\sin\theta_{0V}/\sin\theta_{0T})^{1/2} = 1.092$ from (8).

Gnyloskurenko et al. [14] and Byakova et al. [15] find that the volume of the bubble increases with θ_0 for hydrophobic surfaces of acrylic plastic coated with vacuum silicon grease and paraffin. This is at variance with our results here. In an attempt to approximate the conditions of the experiments of refs. [14,15], we have repeated some of our experiments removing the long capillary that was used to ensure a constant volumetric flow rate. The time histories of the volume of the attached bubble, $V(t)$, reveal that the flow rate is not a constant in the absence of the capillary. Some of these histories are similar to the histories reported in refs. [14,15], displaying an initial waiting phase of very small dV/dt, followed by a short phase of high dV/dt, and a longer final phase of moderate growth rate. Furthermore, the time variation of the radius of the contact line is more pronounced when the capillary is removed than it is in Fig. 3b and c above, and the contact angle varies with time accordingly ref. [21]. For a given value of the time averaged flow rate ($\tilde{Q} = T^{-1}\int_0^T Q(t)dt$, where T is the bubbling period), the final volume is always larger when the flow rate varies with time than when it is a constant, and the final volume may moderately increase with θ_0 on hydrophobic surfaces in the former case. This evidence suggests that the discrepancy between our results of Section 3 for constant flow rate and the results of refs. [14,15] may be due to the time dependence of the rate of growth of the bubble in refs. [14,15]. Particularly striking is the fact that the radius of the contact line and the Contact angle are nearly constant during most of the bubbling period when the flow rate is kept constant, a result already noticed in ref. [18]. While we cannot offer at present a physical explanation of this result, we have used it as a basis of a simple model that approximately reduces our results for different wetting conditions to a single volume/flow rate relationship.

5. Conclusions

In this work we have reported a series of controlled experiments on the growth and detachment of non-spherical bubbles from an orifice at the bottom wall of a liquid under constant gas flow rate conditions. These experiments are aimed at describing the influence of wetting conditions for hydrophilic and hydrophobic surfaces. They have been carried out for accurately controlled constant volumetric flow rates in the range $0.5\,\text{mm}^3/\text{s} \le Q \le 1.33 \times 10^4\,\text{mm}^3/\text{s}$, several radii of the injection orifice, and three static contact angles in the range $68^\circ \le \theta_0 \le 123^\circ$.

The results can be summarised as follows:

1. The capillary system used in the experimental setup provides an accurate and constant volumetric flow rate.
2. All data fit approximately a single curve when a properly scaled bubble volume at detachment is plotted versus a properly scaled volumetric flow rate. Well-known results for bubble injection from needles become approximately applicable to injection from orifices in hydrophobic surfaces when these scales are used.
3. A simple model of the bubble shape at detachment is proposed that gives results in good agreement with our experiments at small flow rates. The model predicts that a maximum bubble volume is attained in the quasistatic regime when the static contact angle is $\theta_0 = 90^\circ$, and allows to estimate the volume of the bubble at detachment for any constant flow rate.
4. The experimental results also allow to infer information on the growth and detachment of bubbles which could be useful when dealing with molten metals and other problems where wetting conditions are an issue.

Acknowledgments

The authors acknowledge support of the Spanish Ministerio de Educación y Ciencia through project DPI2002-04550-C07-05 and through programme SAB2002-0137, which allowed a sabbatical stay of one of us (A.M.) in Madrid.

References

[1] R. Kumar, N.R. Kuloor, Adv. Chem. Eng. 8 (1970) 255.

[2] R. Clift, J.R. Grace, M.E. Weber, Bubbles, Drops and Particles, Academic, New York, 1978.
[3] S.S. Sadhal, P.S. Ayyaswamy, J.S. Chung, Transport Phenomena with Drops and Bubbles, Springer-Verlag, Berlin, 1997 (Chapter 7).
[4] S.D. Lubetkin, Bubble nucleation and growth, in: D.J. Wedlock (Ed.), Controlled Particle, Droplet and Bubble Formation, Butterworth-Heinemann, Oxford, 1994 (Chapter 6).
[5] B.K. Mori, W. Douglas Baines, Int. J. Heat Mass Transfer 44 (2001) 771.
[6] M.S. Longuet-Higgins, B.R. Kerman, K. Lunde, J. Fluid Mech. 230 (1990) 365.
[7] J.F. Davidson, B.O.G. Schuler, Trans. Inst. Chem. Eng. 38 (1960) 335.
[8] H. Tsuge, Hydrodynamics of bubble formation from submerged orifices, in: N.P. Cheremisinoff (Ed.), Encyclopedia of Fluid Mechanics, vol. 3, Gulf Publishing Company, Houston, 1986.
[9] W.V. Pinczewski, Chem. Eng. Sci. 36 (1981) 405.
[10] R.B.H. Tan, I.J. Harris, Chem. Eng. Sci. 41 (1986) 3175.
[11] T.G. Leighton, K.J. Fagan, J.E. Field, Eur. J. Phys. 12 (1991) 77.
[12] H.N. Oguz, A. Prosperetti, J. Fluid Mech. 257 (1993) 111.
[13] J.-L. Liow, N.B. Gray, Chem. Eng. Sci. 43 (1988) 3129.
[14] S.V. Gnyloskurenko, A.V. Byakova, O.I. Raychenko, T. Nakamura, Colloids Surf. A 218 (2003) 73.
[15] A.V. Byakova, S.V. Gnyloskurenko, T. Nakamura, O.I. Raychenko, Colloids Surf. A 229 (2003) 19.
[16] P.G. de Gennes, F. Brochard-Wyart, D. Quéré, Capillarity and Wetting Phenomena, Springer Verlag, Berlin, 2004 (Chapter 4).
[17] A. Marmur, E. Rubin, Chem. Eng. Sci. 31 (1976) 453.
[18] D. Gerlach, G. Biwas, E. Durst, V. Kolobaric, Int. J. Heat Mass Transfer 48 (2005) 425.
[19] A. Mamur, E. Rubin, Chem. Eng. Sci. 28 (1976) 1455.
[20] F.J. Higuera, A. Medina, Eur. J. Mech. B/Fluids 25 (2006) 164.
[21] G.E.P. Elliot, A.C. Riddiford, J. Colloid Interface Sci. 23 (1967) 389.
[22] E.B. Dussan, V. Ann. Rev. Fluid Mech. 11 (1979) 371.
[23] W. Fritz, Phys. Z. 36 (1935) 379.
[24] B. Kabanov, A. Frumkin, Z. Phys. Chem. A 165 (1933) 433.